Improvements in the processing of large grain, bulk Y–Ba–Cu–O superconductors via the use of additional liquid phase

You may also be interested in:

Improvements in the processing of large grain, bulk Y–Ba–Cu–O superconductors via the use of additional liquid phase

Jasmin V J Congreve, Yunhua Shi, Anthony R Dennis, John H Durrell and David A Cardwell

Department of Engineering, University of Cambridge, Cambridge CB2 1PZ, UK

E-mail: jvjc2@cam.ac.uk

CrossMark

Abstract

A major limitation to the widespread application of Y–Ba–Cu–O (YBCO) bulk superconductors is the relative complexity and low yield of the top seeded melt growth (TSMG) process, by which these materials are commonly fabricated. It has been demonstrated in previous work on the recycling of samples in which the primary growth had failed, that the provision of an additional liquid-rich phase to replenish liquid lost during the failed growth process leads to the reliable growth of relatively high quality recycled samples. In this paper we describe the adaptation of the liquid phase enrichment technique to the primary TSMG fabrication process. We further describe the observed differences between the microstructure and superconducting properties of samples grown with additional liquid-rich phase and control samples grown using a conventional TSMG process. We observe that the introduction of the additional liquid-rich phase leads to the formation of a higher concentration of Y species at the growth front, which leads, in turn, to a more uniform composition at the growth front. Importantly, the increased uniformity at the growth front leads directly to an increased homogeneity in the distribution of the Y-211 inclusions in the superconducting Y-123 phase matrix and to a more uniform Y-123 phase itself. Overall, the provision of an additional liquid-rich phase improves significantly both the reliability of grain growth through the sample thickness and the magnitude and homogeneity of the superconducting properties of these samples compared to those fabricated by a conventional TSMG process.

Keywords: top seeded melt growth, YBCO, Y-211, microstructure, liquid rich phase, bulk high temperature superconductor, Y-123 matrix

(Some figures may appear in colour only in the online journal)

1. Introduction

Single grain, (RE)-Ba–Cu–O [(RE)BCO, where RE is a rare earth element or Y], bulk high temperature superconductors, have the ability to trap large magnetic fields that are typically more than an order of magnitude larger than those generated by conventional permanent magnets [1]. As a result, there is a wide range of potential applications for these materials, which include levitation devices, such as Maglev trains, energy storage flywheels, rotating machines, such as motors and generators, and trapped flux devices [2–4].

The presence of poorly connected grain boundaries in (RE)BCO superconductors reduces significantly the flow of supercurrent within the bulk microstructure, which, in turn, results in a significant reduction in the size of the current loop and therefore the magnitude of the trapped field generated by the sample [5, 9]. As a result, these materials are only useful for practical applications when processed in the form of large, single grains [6–8]. Top seeded melt growth (TSMG) is one of two processes used widely to fabricate YBCO in this form

[5, 10]. TSMG involves heating a precursor powder pellet above the peritectic decomposition temperature of the constituent superconducting $YBa_2Cu_3O_{7-\delta}$ (Y-123) phase, which decomposes into a secondary Y_2BaCuO_5 (Y-211) solid phase and a Ba–Cu–O liquid phase. Slow, controlled undercooling in the presence of a suitable seed crystal enables the nucleation and growth of a large single grain, comprising a superconducting Y-123 phase matrix that contains discrete, non-superconducting Y_2BaCuO_5 (Y-211) phase inclusions that provide effective flux pinning [5, 6, 11].

The peritectic reaction for YBCO on solidification occurs at approximately 1000 °C, and is described as follows [12];

$$Y_2BaCuO_5 + Ba_3Cu_5O_8 \,(liquid) \rightarrow YBa_2Cu_3O_{7-\delta}$$
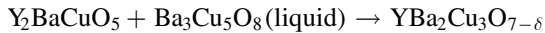
A similar process can be employed using a range of rare earth elements, including Nd, Sm and Gd, rather than Y.

A uniform distribution of small inclusions and defects, including Y-211 inclusions, ideally of size comparable to the coherence length of the Cooper pairs at a given temperature, needs to be present in the Y-123 superconducting matrix to act as flux pinning sites if the single grain samples are to exhibit optimum superconducting properties [6, 13, 14]. Both the distribution and size of the Y-211 inclusions are influenced significantly by the TSMG processing conditions. In general, the distribution of Y-211 inclusions within the Y-123 phase matrix after solidification, which generally increases with increasing distance from the seed, can be modeled by particle pushing and trapping theory [15]. The amount of local undercooling also determines the critical radius of the Y-211 particles trapped at each location within the growing single grain, provided that the Y-211 particles can be considered reasonably as inert [15]. Extended exposure at elevated temperature during the TSMG process results in an undesirable coarsening of the Y-211 particles within the melt, which may be modeled by Ostwald ripening theory. The coarsening of the Y-211 particles is governed by both diffusion of solute through the liquid and the reaction at the interface between the Y-211 particle and the liquid-phase [16]. Therefore, the chemical composition of a single grain fabricated by TSMG is generally inhomogeneous due to the complexity of the growth process and outflow of liquid from the sample during grain growth [16, 17].

Infiltration and growth (IG) is an alternative technique used to fabricate large, single grain bulk (RE)BCO superconductors. Typically, this involves arranging a pressed RE-211 preform pellet above a liquid-rich source pellet. Upon heating, the RE-211 pellet remains solid while the liquid-rich source pellet melts, infiltrating upwards into the preform and reacting with the RE-211 phase to form the RE-123 phase, which will subsequently form the superconducting matrix [18]. This technique overcomes directly the issues of RE-211 particle coarsening and inhomogeneity associated with Ostwald ripening and particle pushing and trapping, since the preform does not melt in the IG method. However, this process is more challenging and complex than TSMG to apply reproducibly, and has only been used relatively recently to fabricate samples reliably.

A successful recycling process has been developed by Shi *et al* [19], based on both the TSMG [9, 10] and IG process [20, 21]. In this approach, a sample that has failed to grow via a primary TSMG process is provided with additional liquid-rich phase from a liquid-rich source pellet, similar to that used in the IG process, to replenish liquid lost during the initial, or primary, melt process. The additional liquid-rich phase is able to infiltrate into the failed grain upon heating to form additional RE-123 phase at the growth front [19]. This provides a sufficient concentration of the respective rare earth element at the growth front to enable a single grain to grow more easily by providing a more uniform composition at the growth front [22].

The recycling process has been observed to be more reliable in the successful fabrication of single grain samples than the primary TSMG process. Recycled samples typically exhibit extended through-thickness grain growth and a much more uniform and homogeneous distribution of RE-211 particles throughout the sample microstructure, which is considered to be due directly to the provision of additional liquid-rich phase [22]. Additional liquid-rich phase was incorporated in the TSMG process for the fabrication of YBCO single grains in this study in an attempt to improve the reliability of complete sample growth and to produce a single grain sample with a highly uniform distribution of RE-211 particles and, therefore, more uniform and potentially improved superconducting properties. A much smaller quantity of additional liquid-rich phase was used in the fabrication of these samples than in the recycling technique.

The microstructure and properties of the samples fabricated with additional liquid-rich phase were compared with samples produced by the conventional TSMG technique. The superconducting properties of both sets of samples were measured and compared along the *c*-axis direction of each single grain, in addition to the microstructure and composition along both the *a* and *c*-axes. The trends in the distribution of the Y-211 and Y-123 phases and the effect of the additional liquid-rich phase at both the top and bottom surfaces and through the thickness of the single grain samples are observed. Conclusions have been drawn on the effect of the provision of additional liquid-rich phase on samples fabricated by the TSMG process.

2. Method

2.1. Buffer aided TSMG and TSMG with additional liquid-rich phase

Two samples were grown by conventional TSMG [5, 20] and nine samples were provided with additional liquid-rich phase in an incremental growth optimization process. Three liquid-rich phases were investigated, of which the optimum composition was identified to be $Yb_2O_3 : Ba_3Cu_5O_8 : BaO_2$ in a molar ratio of 5.0 : 5.6 : 1.0. These precursor powders were calcined once at 850 °C for 5 h prior to melt processing. Yb was chosen as the RE element within the liquid-rich phase to prevent the formation of subgrains at the bottom as the Yb-
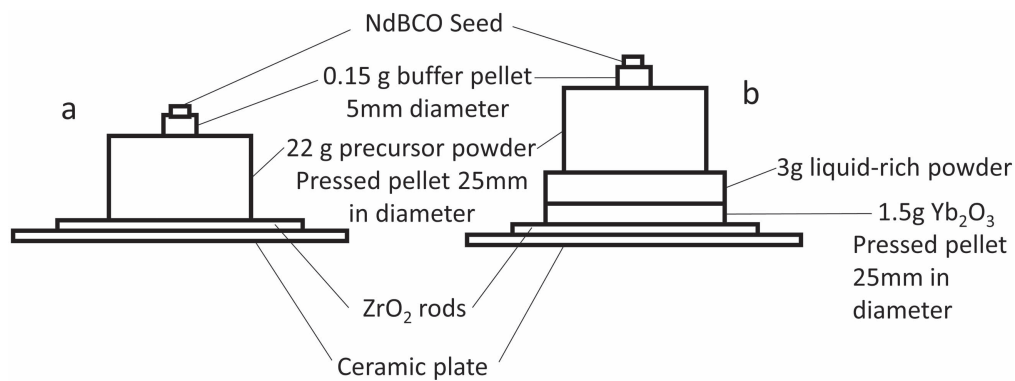
Figure 1. Sample assembly for melt processing: (a) sample 1 by conventional TSMG and (b) sample 2 by TSMG with additional liquid-rich phase.

based liquid-rich phase has a lower melting temperature than Y-123.

The growth of a standard sample fabricated by the conventional TSMG process employed a cylindrical precursor powder pellet of composition 75 wt% Y-123, 25 wt% Y-211 and 0.5 wt% CeO_2 with a mass of 22 g and was pressed uniaxially to a diameter 25 mm. A buffer pellet of diameter 5 mm diameter of mass 0.15 g was placed at the center of the top surface of the green pellet and a NdBCO seed was placed centrally on top of the buffer pellet. A layer of Yb_2O_3 was painted onto the bottom surface of the precursor powder pellet to reduce the likelihood of satellite grain nucleation at the ZrO_2 rods used to support the entire precursor sample arrangement.

The additional liquid-rich phase was provided by 3 g of powder pressed into a pellet of diameter 25 mm with a 1.5 g layer of Yb_2O_3 powder incorporated at its base to provide a mechanically stabilizing layer. This double layer powder pellet was placed between the precursor powder pellet and the ZrO_2 rods. The two samples assemblies prior to melt processing are shown schematically in figure 1.

Both sets of samples were heated in air in a box furnace at $100\,°C\,h^{-1}$ to $926\,°C$, held there for 4 h, heated at $50\,°C\,h^{-1}$ to $1046\,°C$, held for 1 h, cooled at $50\,°C$ to $1001\,°C$, cooled at $1\,°C\,h^{-1}$ to $996\,°C$, cooled at $0.4\,°C\,h^{-1}$ to $970\,°C$ and, finally, cooled at $100\,°C\,h^{-1}$ to room temperature. The samples were annealed following melt processing in a tube furnace in an oxygen-rich atmosphere at $450\,°C$ for 8 d to enable the transformation of the Y-123 matrix from a non-superconducting tetragonal to a superconducting orthorhombic structure. It should be noted that the precision of the temperatures and timings during the various stages of the TSMG process are critical for the production of a large, single grain sample.

Photographs that are typical of the two samples investigated are shown in figure 2. These may be identified as single grains by the four-fold facet lines, exhibited on the top surface and extending down the sides of each sample. Sample 1 was grown by a conventional buffer aided TSMG process, whereas sample 2 was also grown by a buffer aided TSMG process but provided with additional liquid-rich phase of the composition indicated above. The single grain region of

sample 2 was observed to extend to the base of the sample, whereas that in sample 1 did not and contained a number of small, secondary grains in its microstructure. Figure 3 shows the central cross section of both samples, secondary grains can be seen at the base of sample 1 in figure 3(a).

2.2. Measurement of superconducting properties

2.2.1. Trapped magnetic field. Unreacted liquid-rich phase was removed from the base of sample 2 before the top and bottom surfaces of both samples were polished flat and parallel. The maximum trapped magnetic fields at both the top and bottom of the samples were measured at 77 K following field cooling in an applied magnetic field of 1.4 T. The magnetic field was measured initially using a hand-held Hall sensor positioned 0.5 mm above each sample surface. The full trapped field profiles at both the top and bottom surfaces were then measured using a rotating array of 20 Hall probes at a distance of 1.0 ± 0.5 mm from the surface of each sample.

2.2.2. Transition temperature (T_c) and critical current density (J_c). Samples 1 and 2 were cut in half along a diameter to expose a rectangular cross section and cut further into sub-specimens of approximate dimensions $1.5\,mm \times 2.0\,mm \times 1.2\,mm$, as shown schematically in figure 4. These samples were then analyzed using a SQUID (superconducting magnetic interference device) magnetometer (Quantum Design MPMS XL). The value of T_c was established directly from the measured data at a constant field of $1.6\,kA\,m^{-1}$ and the value of J_c at 77 K was derived from the observed hysteresis loops using the extended Bean model [23].

2.3. Microstructure and composition

The samples were imaged using an optical microscope, at a magnification of 50x to observe the pore and crack distribution and at 1000x magnification to observe the Y-211 size and distribution. Images were taken at intervals of 1 mm along both the a and c-axes of the single grain samples. The a/b-axis (i.e. radial) direction of sample 1 was also imaged at a distance 1.5 mm from the base given that the single grain
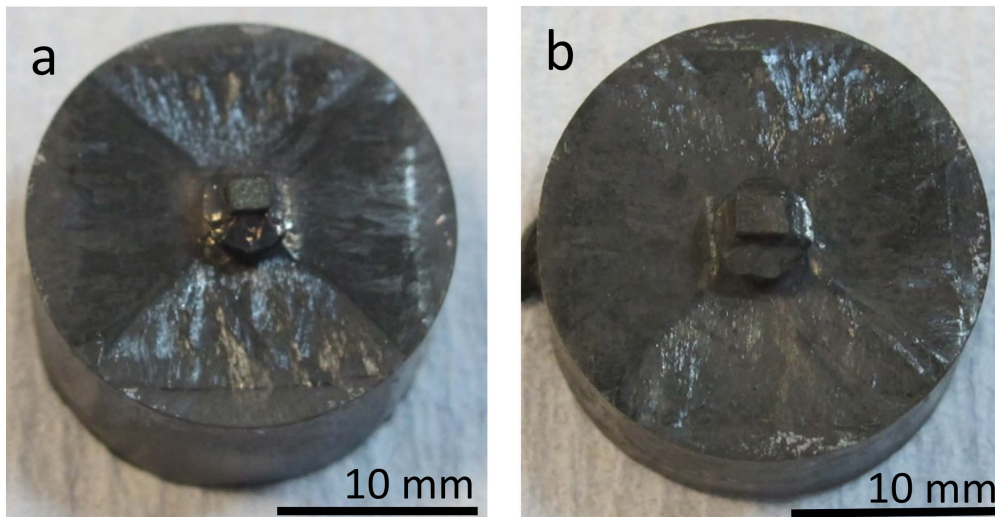
Figure 2. Single grain samples after melt processing: (a) sample 1 and (b) sample 2.
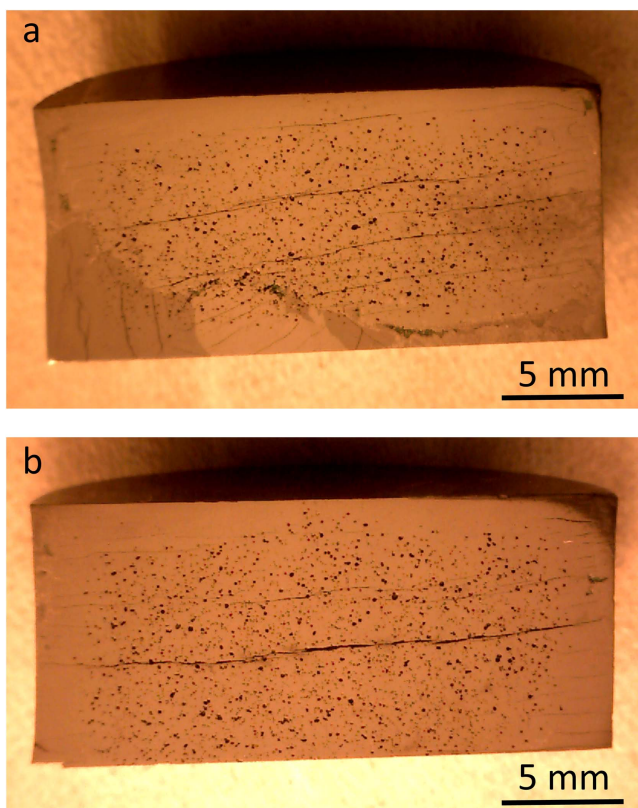

Figure 3. Low magnification images of the central cross section of (a) sample 1 and (b) sample 2 shows a number of secondary grains nucleated from the base of sample 1.

Figure 4. A schematic representation showing: (a) the locations of the various sub-specimens and (b) the orientation of the axes imaged within the single grain.

region of did not extend fully to the bottom of this sample. This enabled the microstructure at the bottom of the single grain region to be studied. The orientation of the single grain axes is illustrated in figure 4(b). The microstructure of the two samples was also observed for areas of approximately 40 μm $\times$ 40 μm at intervals of 1 mm using a scanning electron microscope (SEM), at 2000x magnification with an acceleration voltage of 25 kV, along the three regions of the

samples studies using the optical microscope in order to compare the Y-211 distributions and microstructures between equivalent regions and between the two samples themselves. The average composition for each approximate 40 μm $\times$ 40 μm area imaged using SEM was recorded using an energy dispersive x-ray (EDX) spectroscopy analyzer (s-3400).
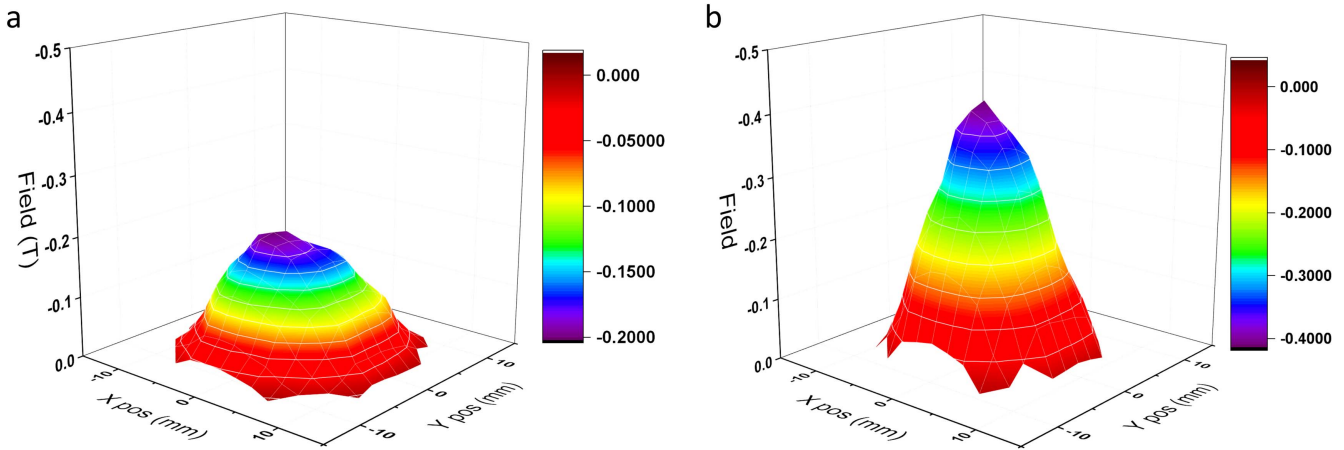
Figure 5. Characteristic trapped field profiles for the base of: (a) sample 1 and (b) sample 2.

The composition data were normalized according to the atomic percentages of Y, Ba and Cu present at each location and the value at each location was compared with the expected stoichiometric atomic percent of Y, Ba and Cu. The differences in composition and variation of composition throughout the two samples were compared in detail. The variation in the calculated ratios of Y:Ba and Y:Cu, which correlate directly with the amount of Y-211 present, were used to identify trends in the distribution of Y-211 inclusions throughout the two samples.

3. Results and discussion

3.1. Superconducting properties

Single grains typically exhibit a characteristic trapped field profile consisting of a single peak that decreases radially and continuously with distance from the seed. Examples of this characteristic trapped field profile at the base of samples 1 and 2 can be seen in figure 5. The maximum trapped field values for the top and bottom surfaces of each of the two samples are given in table 1. The maximum trapped field and the distribution of the trapped field, shown in figure 6, is very similar for both samples on their top surfaces, although the maximum trapped field value at the base of the sample grown using the additional liquid-rich phase is more similar to the maximum value measured at the top surface of both samples. This value of trapped field is significantly higher than that measured at the base of the sample grown without additional liquid-rich phase. The uniformity of the trapped field profile is also much greater for the sample grown with the additional liquid-rich phase than for the sample fabricated using conventional TSMG, as is apparent from the more circular and more uniformly spaced contour lines in figure 6(d).

The measurement of magnetization with varying temperature is shown in figure 7. Very little variation in T_c was observed throughout the samples, as expected for single grain YBCO, or between the samples, with all values of T_c lying in the range 90.6 ± 0.2 K for both samples.

Table 1. Maximum values of trapped field measured at the top and bottom surfaces of samples 1 and 2.

Sample	Maximum trapped field (T)		
	Top	Bottom	Difference
1	0.532	0.262	0.270
2	0.596	0.548	0.048

An additional parameter, ΔT, defined as the temperature range within which 90% of the magnetic moment is observed and which corresponds roughly to a measurement of transition width using a resistive technique, can be used to characterize the quality of the single YBCO grain. It can be seen that the variation in ΔT is larger between sub-specimens and between samples than the actual value of T_c. In addition, it is apparent from the relatively shallow gradient of the transition in figure 7(a) that the value of ΔT increases with increasing distance from the seed for both samples and then decreases at the bottom of sample 2. Unfortunately, the sub-specimen corresponding to position 1te in the single grain could not be analyzed for sample 1, since this was outside the single grain region (this sample had not fully grown to its base). The distribution in ΔT and the trend in the trapped field profiles suggest that the provision of additional liquid-rich phase to sample 2 has a significant effect on improving the quality and uniformity of superconducting properties at the bottom of the sample.

J_c as a function of magnetic field was calculated for each of the sub specimens from the magnetic moment hysteresis curves, as shown in figure 8. It can be seen that sample 1 exhibits a much larger variation in the distribution of the J_c data. The value of J_c is higher for all sub-specimens in sample 2 than in sample 1, with the exception of location 1tc. Both samples show a trend of increasing J_c with distance from the seed until position 1tc in the single grain microstructure, and at which point J_c decreases with increasing distance from the seed.

Sample 2 exhibits much less variation in J_c between sub-specimens, and a significantly higher and more uniform
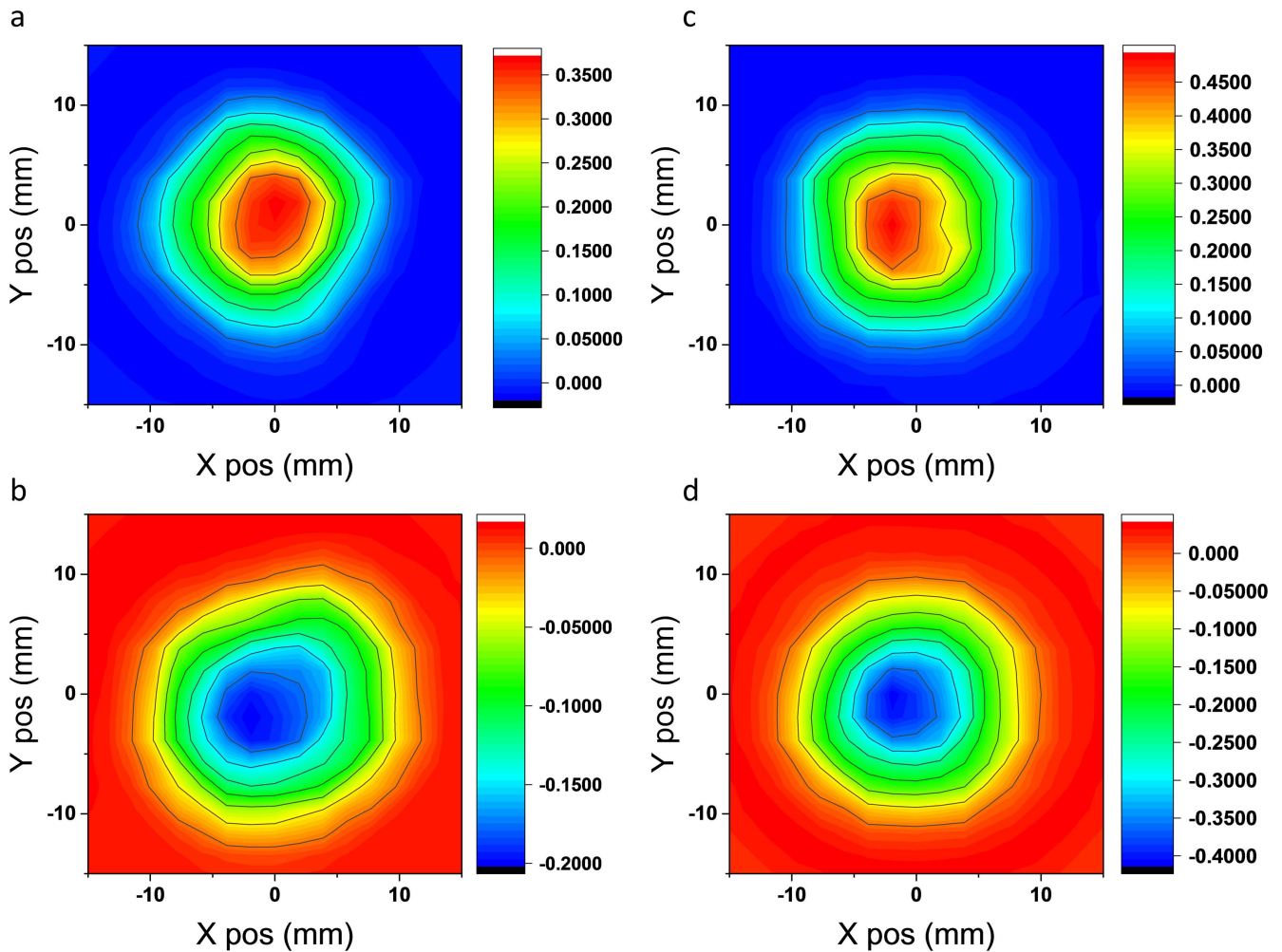
Figure 6. Trapped field distribution for: (a) sample 1 top, (b) sample 1 bottom, (c) sample 2 top and (d) sample 2 bottom.

distribution of the maximum value of J_c for all the sub-specimens along the c-axis, with the exception of sub-specimen 1tc. This suggests that the provision of additional liquid-rich phase produces a much more uniform distribution of flux pinning centers, and therefore a more uniform distribution of the Y-211 precipitates, and a much more uniform distribution of Y-123 superconducting phase than in the sample grown by the conventional TSMG process. This leads directly to more homogeneous superconducting properties throughout the sample and to a significantly greater magnitude of magnetic moment (and potentially trapped magnetic field).

3.2. Microstructural analysis

The presence of Y-211 particles at the top surfaces of both samples was confirmed by EDX analysis, and that the concentration of these particles increased with increasing distance from the seed. This trend has been observed previously in conventional TSMG samples and recycled samples provided with additional liquid-rich phase [15]. This suggests that the provision of additional liquid-rich phase has little effect on the microstructure at the top surface of the sample, indicating possibly that there is insufficient time for the additional liquid-rich phase to infiltrate all the way to the top of the

sample, or that there is already sufficient liquid-rich phase present in this region of the sample and therefore no compositional gradient to drive the infiltration of additional liquid-rich phase to the top surface of the sample.

Images of the samples taken along the c-axis indicated the presence of sub-grains at the base of sample 1, whereas sample 2 was grown fully to the bottom of the precursor pellet. This suggests that the additional liquid-rich phase enables the extension of the growth of the single grain region to the base of the sample, thus producing a larger single grain region and increasing the overall quality of the sample. Both the number of cracks and pores decreases with distance from the seed in the c-axis direction for sample 2, which is not observed in sample 1, which may be due to the additional liquid-rich phase infiltrating into and filling these microstructural features. This results in a sample that contains a larger region of uninterrupted, continuous Y-123 superconducting phase matrix, as is confirmed by the value of magnetic moment observed for the sub-specimen taken closest to the base of sample 2, which has the highest value of J_c at position 1te for the samples under investigation. The distribution of Y-211 inclusions in sample 1, shown in figure 9, is as anticipated from particle pushing/trapping theory for all
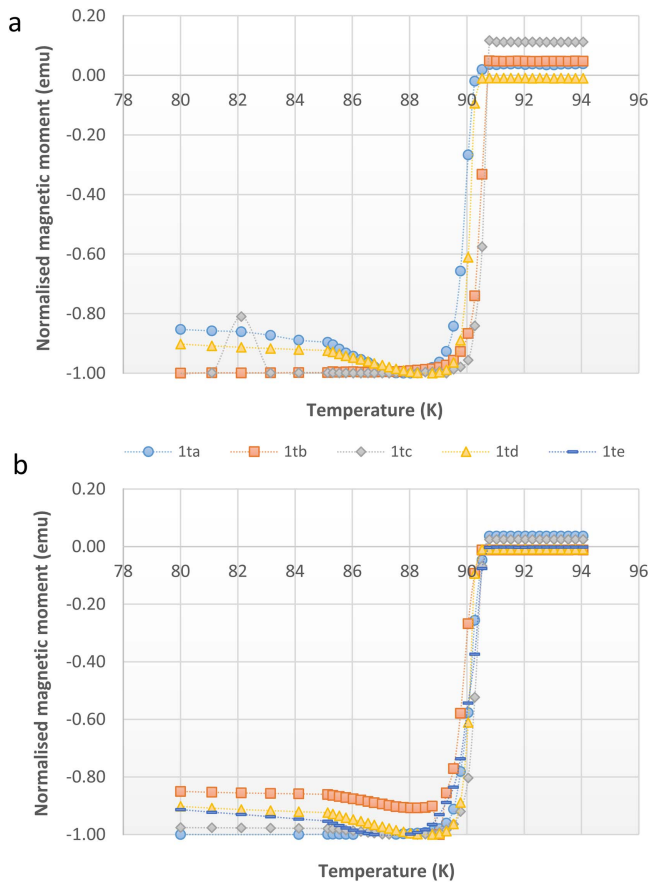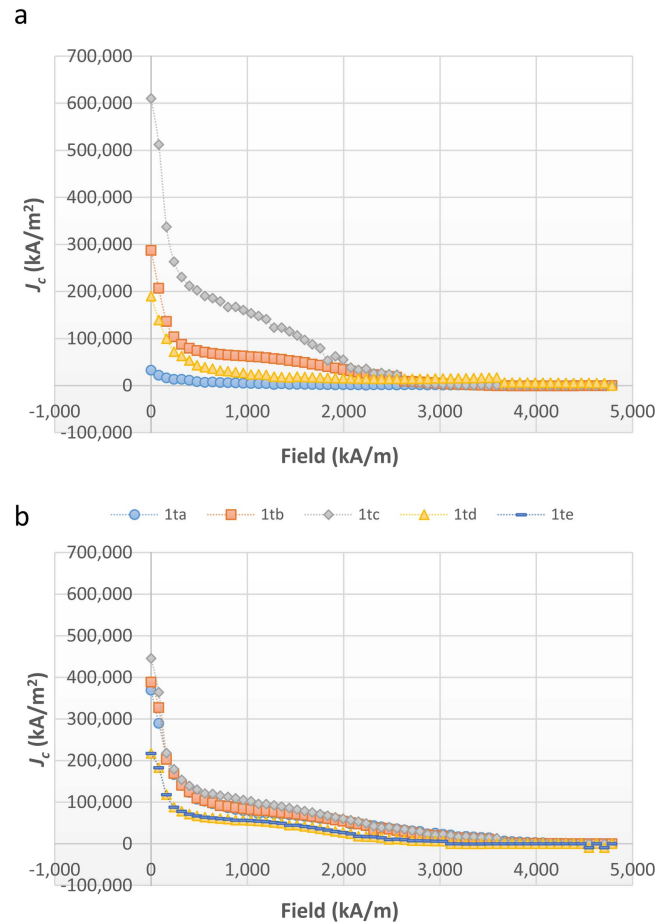
Figure 7. Magnetic moment as a function of temperature used to determine T_c for (a) sample 1 and (b) sample 2.

Figure 8. Magnetic field dependence of J_c determined from magnetic hysteresis for (a) sample 1 and (b) sample 2.

the images. This predicts that the volume fraction occupied by Y-211 particles increases with increasing distance from the seed, with a larger number of smaller particles being trapped, also with increasing distance from the seed. The distribution of Y-211 inclusions in sample 2 is as anticipated from particle pushing/trapping theory for images a–c, but, due to the provision of additional liquid-rich phase, there are fewer Y-211 inclusions at location d and, therefore, a greater concentration of the superconducting Y-123 phase. This suggests that the provision of additional liquid-rich phase increases the uniformity of the Y-211 inclusions and Y-123 matrix towards the base of the sample.

3.3. Compositional analysis

Measurement of the average composition of areas approximately $40 \, \mu$m $\times$ $40 \, \mu$m at intervals of 1 mm throughout the bulk single grain samples has indicated that the average composition at each location tends to fluctuate around the expected stoichiometric composition for both samples.

Figure 10 shows variations in primary elemental composition in samples 1 and 2 for all three directions imaged (horizontally across the top corresponding to the a/b-axis, horizontally across the base corresponding to the a/b-axis and vertically through the thickness corresponding to the c-axis).

It can be seen that both samples show similar trends of decreasing normalized Cu at% (atomic percentage), almost constant normalized Ba at% and increasing normalized Y at% with increasing distance from the seed. These values correlate with the amount of liquid-rich phase ($Ba_3Cu_5O_8$) present and indicate that the amount of this present at each location reduces with increasing distance from the seed in both samples. Sample 1 exhibits much larger fluctuations in the normalized compositions and a steeper general trend in their variation than sample 2 in both the vertical and horizontal directions along the base of the samples. This suggests that there is a greater variation and reduction of liquid phase in the vertical direction and at the base of sample 1 than sample 2. It appears that the liquid-rich phase only infiltrates part of the way up the sample and has little effect on the composition at the top of the sample, since the magnitude of the fluctuations in composition are similar and the gradient in the general trend in the observed decrease in the normalized atomic percentages is similar at the top surfaces of both samples.

EDX analysis enabled the location of the edge of the single grain region to be identified from the normalized composition plots as the point where the normalized concentrations of Cu and Y begin to strongly converge, as shown
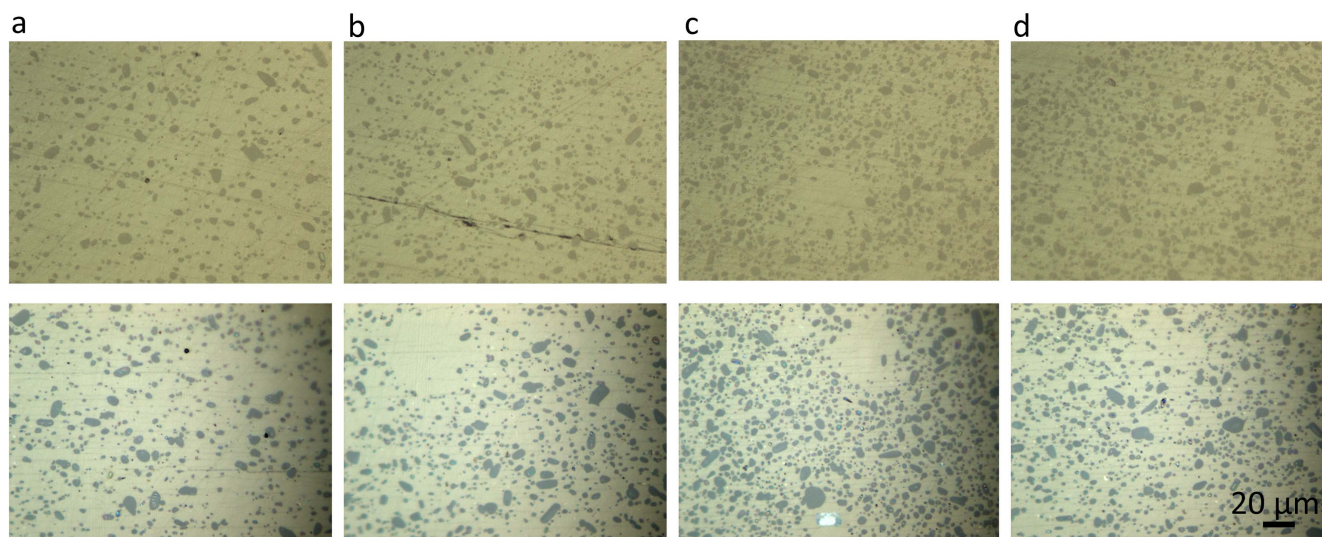
Figure 9. Optical microscope images with increasing distance from the seed in the *c*-axis direction at 1000x magnification at positions of (a) 0 mm, (b) 2 mm, (c) 5 mm and (d) 6 mm. The top and bottom rows correspond to samples 1 and 2, respectively.

in figure 10. This occurs at 11 mm along the top surface in sample 1 and corresponds directly with the images taken using SEM, from which the edge of the single grain region can be identified visually.

The ratios of Y:Ba and Y:Cu correlate directly with the amount of Y-211 present locally in the sample microstructure. As a result, the average ratio for each area over which the composition was measured and the variation in composition ratio were used to identify the trend in the distribution of Y-211 inclusions throughout the two samples. Plots of these ratios for both samples are shown in figure 11. Both Y:Ba and Y:Cu ratios increase with increasing distance from the seed along all three directions investigated. This suggests that the amount of Y-211 increases with increasing distance from the seed throughout each sample. However, sample 1 exhibits both a greater increase in both ratios with increasing distance from the seed and wider fluctuations than sample 2, except at the top of the sample, with the greatest differences being particularly pronounced in the vertical direction. This suggests that the additional liquid-rich phase provided has no effect on the distribution of Y-211 at the top of the sample, although the amount of Y-211 does increase with distance from the seed as it does in the other directions. The additional liquid-rich phase provided during the growth process does have a noticeable effect upon the ratio of Y-211 to Y-123 particles lower down the sample, with the additional liquid-rich phase provided enabling an increased uniformity in the distribution of Y-211 particles towards the base of the sample. This, therefore, increases the uniformity in the amount of the Y-123 superconducting phase within which the supercurrent can circulate. (It should be noted that microscope images do not indicate a sudden fluctuation in the amount of Y-211 inclusions at the edge of the grain, as is observed in the graph in figure 11 for the horizontal direction.)

3.4. Relation between microstructure, composition and superconducting properties

The liquid-phase carries the Y element with it in the peritectically decomposed state and so the presence of additional liquid-rich phase enables an additional and sufficient quantity of Y to be transported to the growth front of the sample during the single grain growth process. This suggests that provision of additional liquid-rich phase enables the peritectic reaction to continue to the edge of the sample, and, without which, growth of the complete sample would otherwise be incomplete. As a result, the additional liquid-phase, and specifically the concentration of Y that it transports, is able to provide a more uniform composition at the growth front and, as such, enables more reliable growth and an extended growth region given that the growth of a single grain is limited by diffusion of the Y element at the growth front.

The composition at the growth front has a much greater uniformity than the bulk of the sample. As a result, the regions within the bulk sample to which the additional liquid is able to infiltrate to provide the extended growth effect, which are predominately the base of the sample but include, to some extent, the entire sample, exhibit a much greater uniformity in the Y-211 particle distribution than for samples grown by conventional TSMG. The composition at the base and at a distance over 3 mm from the seed along the *c*-axis direction is much more uniform due to the presence of additional liquid and, therefore, the presence of additional Y at the growth front.

Microstructural studies of samples produced by the conventional TSMG process reveal that the amount of liquid phase present during grain growth decreases with increasing distance from the seed, and exhibits larger fluctuations between adjacent locations within the single grain structure. The large decrease towards the base of the sample is likely to be due to the loss of liquid during melt processing, and this is more significant at the bottom of the sample. The increased
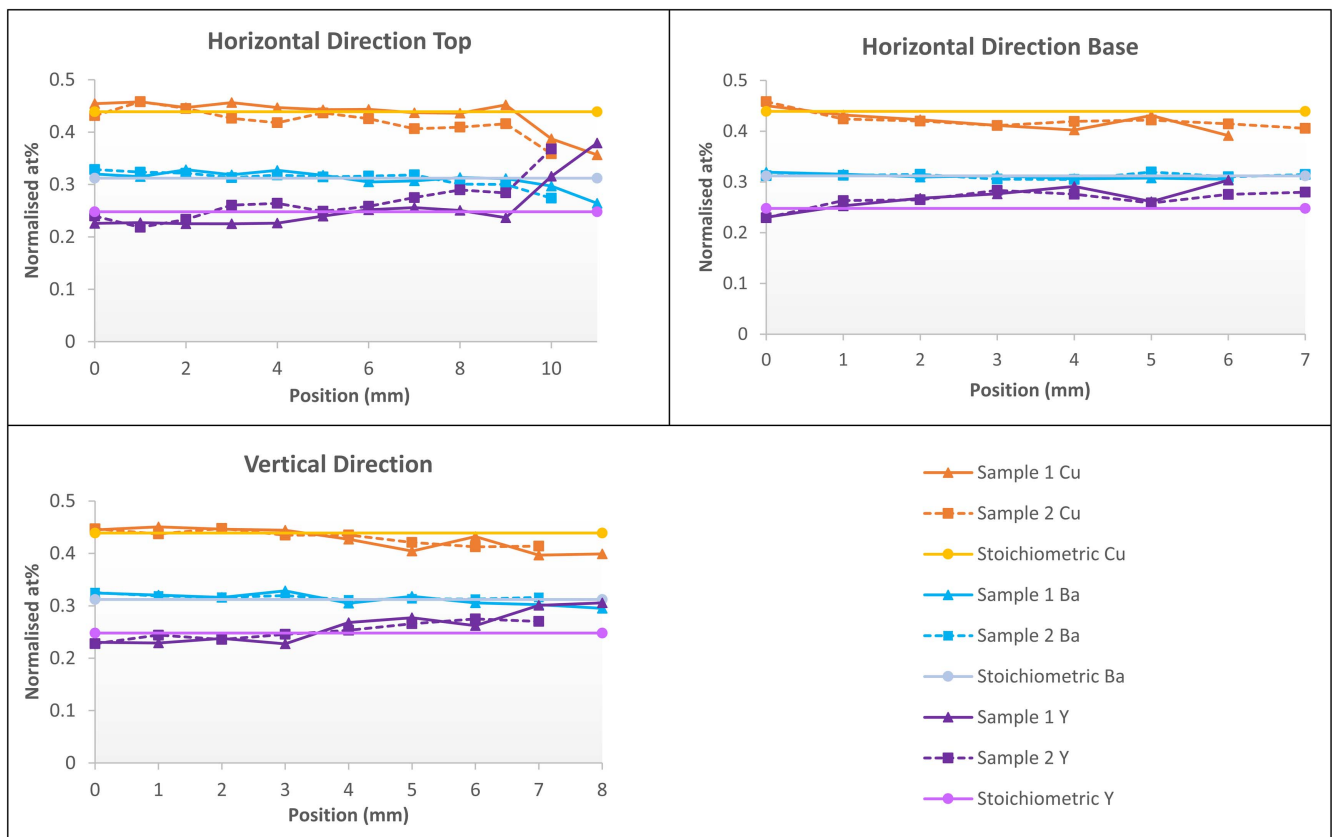
Figure 10. The variation of normalized composition with position for samples 1 and 2.

uniformity of the liquid phase distribution and the higher levels of liquid phase present in the sample grown with additional liquid-rich phase are attributed to the ability of the additional liquid-rich phase to infiltrate upwards into the pressed precursor pellet. The most prominent effects on the composition are observed towards the base of the sample. Comparison of the two samples studied here has shown that the provision of additional liquid-rich phase has relatively little effect on the top surface of the single grain. This suggests, therefore, that less liquid is lost from the top of the sample during conventional TSMG than it is from the base. Homogeneous nucleation during the growth process occurs at the seed on the top surface of the sample, as a result, the top surface of the sample is the first to solidify, so initially there is sufficient liquid phase and local Y content to produce a single grain with a uniform composition and microstructure. As solidification proceeds, however, the amount of liquid phase, and therefore the amount of Y being supplied to the growth front, decreases with increasing distance along the *c*-axis of the sample. In turn, this reduces the uniformity of the composition and the distribution of Y-211 inclusions within the Y-123 phase matrix. No significant change in the composition, uniformity of composition, distribution of liquid phase or the concentration of Y-211 at the top of the sample occurs compared to that observed in a single grain fabricated by conventional TSMG when additional liquid-rich phase is provided because there is already sufficient liquid phase present at the top of the sample.

The small, unreacted Y-211 particles trapped within the Y-123 phase matrix during peritectic solidification create Y-211/Y-123 interfaces that are able to act as effective flux pinning centers. The flux pinning centers determine the ability of the sample microstructure to pin flux, which, in turn, determines the magnitude of the in-field critical current density. The fabrication of a large, connected single grain region is fundamental to the generation of a large trapped field. An increased uniformity of the distribution of Y-211 particles within a given volume fraction range, therefore, is able to account for a larger and more uniform value of J_c, and especially at the base of the sample. However, the volume fraction of the superconducting Y-123 phase will be too low to further increase J_c and trapped field above a critical volume fraction of Y-211 particles.

The increase in uniformity of the trapped field profile at the base of the sample grown with additional liquid-rich phase can be explained generally by the increased homogeneity of the Y-211 distribution throughout the sample microstructure, which results directly in improved homogeneity of flux pinning and to an increased uniformity in the distribution of Y-123 phase throughout the sample. The increase in magnitude of the maximum trapped field measured at the base of the sample provided with additional liquid-rich phase can be explained, at least in part, by the increase in the measured value of J_c as a result of the increased uniformity of the Y-211 inclusion distribution but is probably due predominately to the increase in uniformity and quantity of the Y-123
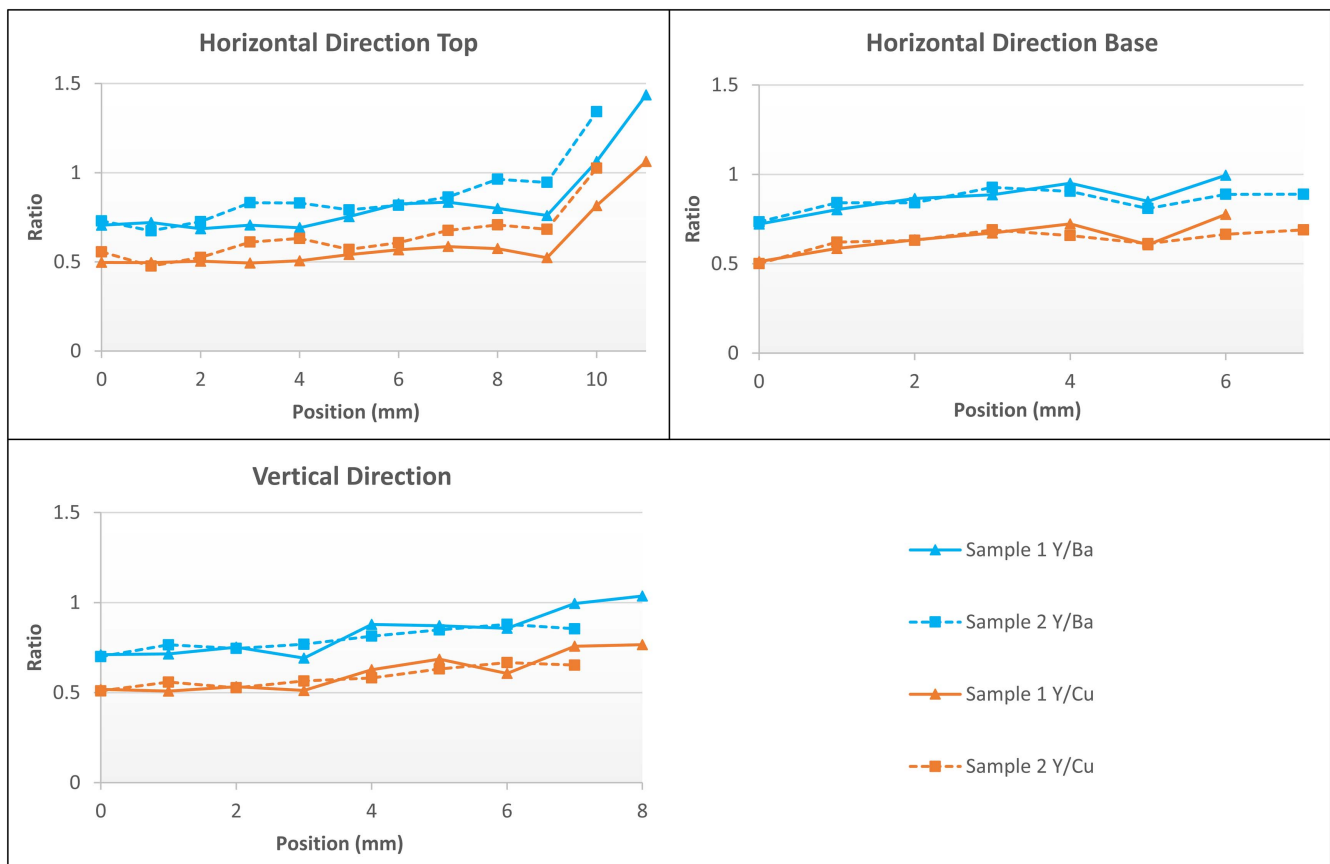
Figure 11. The variation of the ratio of Y:Ba and Y:Cu elemental compositions with position in samples 1 and 2.

superconducting phase in this region of the sample, which generates a larger area over which the superconducting current can flow.

4. Conclusion

The provision of additional liquid-rich phase during the fabrication of YBCO bulk samples by TSMG has been shown to increase significantly the reliability with which through-thickness, single grain growth is obtained compared to samples grown by conventional TSMG. This is due to the fact that the additional liquid-rich phase is able to infiltrate from the source precursor pellet into the lower portion of the sample during the grain fabrication process. Moreover, increased uniformity at the growth front produces a more uniform overall composition in the lower section of the sample, which results in both a greater homogeneity in the distribution of Y-211 particles and an increased uniformity of the Y-123 superconducting phase matrix. This leads to a much greater uniformity in the key superconducting properties, which include T_c, J_c and trapped magnetic field, in large, single grains fabricated using the additional liquid-rich phase technique. We have shown, therefore, that the provision of additional liquid-rich phase during growth is a simple and effective modification to the well-established conventional TSMG process that leads to improved reliability and sample performance.

References

[1] Durrell J H *et al* 2014 A trapped field of 17.6 T in melt-processed, bulk Gd–Ba–Cu–O reinforced with shrink-fit steel *Supercond. Sci. Technol.* **27** 082001
[2] Campbell A M and Cardwell D A 1997 Bulk high temperature superconductors for magnet applications *Cryogenics* **37** 567
[3] Werfel F N, Floegel-Delor U, Rothfeld R, Riedel T, Goebel B, Wippich D and Schirrmeister P 2012 Superconductor bearings, flywheels and transportation *Supercond. Sci. Technol.* **25** 014007
[4] Li B, Zhou D, Xu K, Hara S, Tsuzuki K, Miki M, Felder B and Deng Z 2012 Materials process and applications of single grain (RE)-Ba–Cu–O bulk high temperature superconductors *Physica* C **482** 50–7

[5] Cardwell D A 1998 Processing and properties of large grain (RE)BCO *Mater. Sci. Eng.* **B53** 1–10

[6] Dimos D, Chaudhari P, Mannhart J and Le Goues F K 1988 Orientation dependence of grain-boundary critical currents in YBa$_2$Cu$_3$O$_{7-\delta}$ bicrystals *Phys. Rev. Lett.* **61** 219–22

[7] Todd V R, Zhang X F, Miller D J, St Louis-Weber M and Dravid V P 1996 Controlled growth of bulk bicrystals and the investigation of microstructure-property relations of YBa$_2$Cu$_3$O$_x$ grain boundaries *Appl. Phys. Lett.* **69** 3746–8

[8] Durrell J H, Hogg M J, Kahlmann F, Barber Z H, Blamire M G and Evetts J E 2003 Critical current of YBa$_2$Cu$_3$O$_{7-\delta}$ low-angle grain boundaries *Phys. Rev. Lett.* **90** 247006

[9] Shiohara Y and Endo A 1997 Crystal growth of bulk high-T_c superconducting oxide materials *Mater. Sci. Eng.* **19** 1–86

[10] Sawano K, Morota M, Tanaka M, Sasaki T, Kimura K and Takebayashi S 1991 High magnetic flux trapping by melt-grown YBaCuO superconductors *Japan. J. Appl. Phys.* **30** L1157–9

[11] Namburi D K, Shi Y, Palmer K G, Dennis A R, Durrell J H and Cardwell D A 2016 An improved top seeded infiltration growth method for the fabrication of Y–Ba–Cu–O bulk superconductors *J. Eur. Ceram. Soc.* **36** 615–24

[12] Fujimoto H, Murakami M, Gotoh S, Koshizuka N, Oyama T, Shiohara Y and Tanaka S 1990 Melt processing of YBaCuO oxide superconductors *Advances in Superconductivity: II. Proceedings of the 2nd International Symposium on Superconductivity* (Japan: Springer) pp 285–8

[13] Krabbes G, Fuchs G, Canders W R, May H and Palka R 2006 *High Temperature Superconductor Bulk Materials Fundamentals—Processing—Properties Control—Application Aspects* (Weinheim: Wiley-VCH Verlag GmH & Co. KGaA)

[14] Murakami M 1992 *Melt Processed High-Temperature Superconductors* (Singapore: World Scientific)

[15] Diko P 2000 Growth-related microstructure of melt-grown REBa$_2$Cu$_3$O$_y$ bulk superconductors *Supercond. Sci. Technol.* **13** 1202–13

[16] Li B *et al* 2012 Materials process and application of single grain (RE)-Ba–Cu–O bulk high temperature superconductors *Physica* C **482** 50–7

[17] Li G-Z, Dong L and Deng X-Y 2016 Comparisons of the microstructure and superconducting properties in Y–Ba–Cu–O single-grain superconductors grown with different liquid sources: the influence of element doping through liquid infiltration *Ceram. Int.* **42** 923–8

[18] Devendra Kumar N, Shi Y, Zhei W, Dennis A R, Durrell J H and Cardwell D A 2015 Buffer pellets for high-yield, top-seeded melt growth of large grain Y–Ba–Cu–O superconductors *Cryst. Growth Des.* **15** 1472–80

[19] Shi Y, Namburi D K, Wang M, Durrell J, Dennis A and Cardwell D 2015 A reliable method for recycling (Sm, Gd, Y)Ba$_2$Cu$_3$O$_{7-\delta}$ bulk superconductors *J. Am. Ceram. Soc.* **98** 2760–6

[20] Li G-Z, Li D-J, Deng X-Y, Deng J-H and Yang W-M 2013 Infiltration growth and crystallization characterisation of single-grain Y–Ba–Cu–O bulk superconductors *Cryst. Growth Des.* **13** 1246–51

[21] Zhou D, Hara S, Li B, Xu K, Noudem J and Izumi M 2013 Significant improvement of trapped flux in bulk Gd–Ba–Cu–O grains fabricated by a modified top-seeded melt growth process *Supercond. Sci. Technol.* **26** 015003

[22] Congreve J V J, Shi Y H, Dennis A R, Durrell J H and Cardwell D A 2016 Microstructure and composition of primary and recycled single grains of YBCO, GdBCO-Ag, and SmBCO-Ag bulk superconductors *J. Am. Ceram. Soc.* **99** 3111–19

[23] Chen D-X and Goldfarb R B 1989 Kim model for magnetization of type-II superconductors *J. Appl. Phys.* **66** 2489